Closed-form analytical approach for calculating noise contours of directive aircraft noise sources

D. C. Amargianitakis*, R. H. Self †, A. R. Proença‡ and A. P. Synodinos§
Institute of Sound and Vibration Research, University of Southampton, Southampton, Hampshire, SO17 1BJ

A. J. Torija¶
Acoustics Research Centre, University of Salford, Manchester M5 4WT, UK

This paper comes as an update to the simplified airport noise model RANE (Rapid Aviation Noise Evaluator) adding capability of including fully non-isotropic noise sources. RANE v2 is developed as a part of multidisciplinary acoustic assessment of novel aircraft, namely, for vehicles within the Urban Air Mobility sector, in order to produce ground contours around airports and helipads. The model uses three-dimensional noise exposure surfaces around a series of discretised segments that represent the aircraft flightpath. The main inputs are the Noise Radius a function of the sources' Sound Power Level (PWL) which come in the form of Noise-Power-Distance curves, and the source three-dimensional directivity. The directivity function may take analytical or numerical form, allowing for experimental data inputs. This paper demonstrates the use of Spherical Harmonics as a form of directivity function with a closed-form analytical proof for calculating the noise exposure contours. Preliminary results and comparison against the FAA's AEDT module for Helicopter Community Noise indicate that exposure contour coordinates may be estimated with little uncertainty. The incorporation of source directivity allows for the assessment of lateral attenuation, engine installation effects and transition operations (for vertical to horizontal flight and vice versa) via the assumption of individual source directivities and therefore complex noise surfaces. As a consequence of the analytical nature of the model, low computational requirements allows for fast exploration of the design space and parametric studies, with minimal input requirements. RANE v2 is currently being used to assess ground noise of two novel aircraft concepts; 1. a fixed wing fully electric General Aviation aircraft and 2. a Vertical Take-off and Landing (VTOL) enabled rotorcraft.

I. Nomenclature

SYMBOLS

α	Parameter used for calculation of the finite segment correction ΔF
β	Elevation angle of aircraft relative to ground plane
Δx	Displacement in the x dimension as a consequence of the different inclination angles (γ).
Δt	Time increment
$\Delta x, \Delta y$	Displacement in the x and y directions, respectively.
γ	Inclination angle
$\Lambda(\beta)$	Long range air-to-ground lateral attenuation
$\Lambda(\beta, l)$	Lateral attenuation adjustment
ϕ	Depression angle
ψ	Angle of rotation in the horizontal plane
$\mathbf{S}$	Orthogonal matrix
$\mathbf{U}$	$= (u\ v\ w)^T$, position vector
$\mathbf{X}$	$= (x\ y\ z)^T$, position vector
θ	Polar directivity angle
φ	Azimuthal directivity angle
A	Contour area

*PhD Student, ISVR, University of Southampton, Hampshire, SO17 1BJ
†Professor, ISVR, University of Southampton, Southampton, Hampshire, SO17 1BJ
‡Research Fellow, ISVR, University of Southampton, Southampton, Hampshire, SO17 1BJ
§Visiting Academic, ISVR, University of Southampton, Southampton, Hampshire, SO17 1BJ
¶Lecturer in Acoustical Engineering, Acoustics Research Centre, University of Salford, Manchester M5 4WT

A_T	Total noise contour area due to the total of N segments
d	Shortest distance from an observation point to a flight path segment
d_p	Perpendicular distance from an observation point to the flight path (slant distance)
d_λ	Scaled distance
h	Altitude
L	Event sound-level (scale undefined)
l	Perpendicular distance from an observation point to the ground track
L_E	Single event sound exposure level determined from NPD database
$L_{E,ajk}$	Single event noise exposure level contribution from each segment k of each flight track j and for each aircraft a within the fleet.
$L_{eq,T}$	Energy-equivalent sound-level integrated over the period T
L_E	Single event sound exposure level (SEL)
L_{max}	Maximum sound-level during an event
P	Power-setting parameter in NPD variable $L(P, d)$
Q	Distance from start of the segment to closest point of approach
R	Noise Radius
s	Segment length
T_0	Reference time for integrated sound level
v	Airspeed
v_{ref}	Reference airspeed for which NPD data are defined
Λ_y	(Orthogonal) rotation matrix
ini,end	Limits of integration
len	Length of the noise contour
Δv	Duration adjustment

SUBSCRIPTS

0	Baseline Aircraft
a	Aircraft
i	Individual noise source
j	Flight track; individual parameter influencing noise source i
k	Individual flight track segment
m	Number of aircraft movements
n	Common flight track segments for the whole aircraft fleet

COORDINATE SYSTEMS

θ, φ, r	Spherical coordinate system used for NPD flyover procedures and lateral attenuation definition.
d_p, φ, u	Cylindrical coordinate system for each kth flightpath segment
u, v, w	Orthogonal coordinate system with the u axis is aligned with the kth flightpath segment.
X, Y, Z	Common orthogonal coordinate system for all k flightpath segments, Airport system
x, y, z	Orthogonal coordinate system for each kth flightpath segment

II. Introduction

THE aviation industry is reaching a turning point. The advancement of electrical propulsion systems and battery technologies will slowly allow for manufacturers to introduce new hybrid or fully electric designs to the market. These designs encompass everything from large long hall aircraft, to short hall, regional and even urban air taxis. The introduction of these new categories of aircraft, along with the existing increase in air-traffic, impose a very serious problem to the noise impact around airports and urban areas where these novel aircraft will most likely prosper.

Urban Air Mobility (UAM) or Personal Air vehicles is a rising section of the aviation market seeking to provide on demand aviation services and amenities. At the moment a number of hurdles are in the way of this idea "taking-off"; some of those include: aviation safety, airworthiness, operating and maintaining costs, airspace integration, aircraft noise and emissions and finally community acceptance[1]. As UAM aims to fill a market gap, at the same time it enters an entirely new aviation sector. Innovative technologies such as electric propulsion allow for aircraft/rotorcraft to perform operations and manoeuvres never before capable in the aviation world. Unfortunately, along with these capabilities comes a caveat. Regulations and certification procedures for such operations in urban environments (and not) have yet to be defined. Current regulations will have to be amended or even replaced with newly defined ones. The process of defining rules and regulations, and integrating such vehicles in an already existing transport and Air traffic control (ATC) infrastructure forms a complex problem itself. It requires a full understanding of the capabilities of the vehicles along with all risks associated with all engineering components in order for safe operation to be accomplished. Along with the risks, the impact of vehicles on their operation environment must also be understood. In urban areas where people are densely populated, generated noise may strongly influence the regulations decided upon and may greatly affect (or delay) the introduction of UAM vehicles. Therefore the design and prediction capabilities of noise and airport models for these vehicles is a top priority.

The ECAC modelling methodology presented in [2] and the Aircraft Noise and Performance (ANP) database [3] are based around the operation of conventional fixed-wing aircraft. The FAA's Aviation Environmental Design Tool (AEDT) [4] implements this methodology along with extensions to it for a number of civil and military helicopters using an equivalent database that includes helicopter operations (Base of aircraft data, BADA [5]). Although this

methodology allows for the generation of exposure contours around airports and helipads, it is very limited by the inputs and experimental data available. No modularity exists in the definition of noise sources and especially their complex radiation patterns.

The development of electric propulsion systems allows for novel configurations of vehicles. Incorporating distributed electric propulsors along the airframe and wing assemblies; implementing different propulsion systems for vertical and others for horizontal flight; enabling the rotations of propellers, ducted fans and rotors during flight in order for the vehicle to transition from one operating state to another are just some of the many prototypes major manufacturers such as Airbus, Boeing and Bell Helicopters, along with many more smaller enterprises are investigating. In order for a high fidelity tool, such as AEDT or ANCON (Aircraft Noise Contour Model [6]), to make accurate predictions for all novel configurations of vehicles, expensive and time consuming measurement campaigns are required. Sound exposure on the ground, along with aircraft operation and performance data needs to be collected to be used as inputs for the contour generation. Therefore, airport and community noise analysis is postponed until finalised variants of the designs are manufactured and flight tested.

For airport noise and aircraft noise source analysis to be integrated and be part of the preliminary design of these novel aircraft, the restrictive nature of today's tools must be overcome. A modular tool, that allows a variety of inputs; from computational, to experimental even analytical, with the capability of performing many different calculations in short period of time is required. RANE v2 (Rapid Aviation Noise Evaluator), aims to further the capabilities of RANE [7], and move closer to the accomplishment of such a tool.

Although RANE proved that for simple single runway scenarios, changes in airport noise contour areas can be estimated with minimal uncertainty compared against grid-point calculation methods, its main assumption of omnidirectional sources, limits its capabilities to conventional turbofan airliner designs (the dominant turbofan aircraft noise sources contribute to an approximately omnidirectional nature of emission [8]). Furthermore conventional approach, landing, take-off and climb operations are implemented not allowing for the more complex operations such as vertical take-off and landing (VTOL), hovering and mid-air direction reversal. RANE v2 expands the assumption of an isotropic source to the ability to define the aircraft noise source characteristics in more detail. In this paper the source directivity is introduced along with the modifications to the operation definitions in order to accommodate UAM VTOL vehicle calculations.

In this paper the process of developing a closed-form analytical model for the generation of noise exposure contours of highly directive sources around airports is described. The model is based on the work of Stewart and Carson (1979) [9], where the moving aircraft is represented as an axially symmetric noise source, and consequently cylindrical surfaces with constant sound-level are formed around the flight path. The concept of noise exposure surfaces is explicitly defined and their calculation is then performed analytically.

The analytical proofs describing the generation of noise surfaces consider the calculation of the noise impact for an aircraft flying a take-off trajectory, for a single case of totally non-isotropic noise source, $D(\theta, \varphi)$ (although the same derivation could also be performed for isotropic noise sources and directive noise sources in the polar angle only, $D(\theta)$). The Directivity function, D is a measure of the source's directional sound radiation properties and is properly defined later in this report.

The study then continues to detail the process of applying the three-dimensional noise surfaces to a discretised aircraft flightpath during take-off operations of varying nature. The process of converting the noise surfaces to two-dimensional sound exposure contours on the airport plane can be broken down into the following steps:

- Discretisation of continuous flightpath operation into segments of constant parameters.
- Translation and rotation of the contour contributions of each segment onto the common Airport coordinate system.
- Use of quadratic and cubic splines to connect contour segments when discontinuity arises.
- Calculation of area within the contour.
- Finally, dealing with errors due to assumptions made in the analytical calculation of the noise surfaces.

III. Flyover Procedure

A. Current Models and Procedures

The term airport noise describes the science in which the noise due to the cumulative effect of aviation operations is quantified. Contours of different metrics generated around airports and helipads allow manufacturers, government and aviation certification bodies make informed decisions on how noise affects the community around these areas.

Current airport tools base their calculations on experimentally obtained noise data and after a series of interpolations,

extrapolations and corrections provide predictions of noise emissions as a result of aircraft single or cumulative (aircraft fleets) events. The data typically consists of Noise-Power-Distance (NDP) databases generated during the certification process of the aircraft or in many cases individual flyover noise measurement campaigns. NPD curves along with flightpath data are the main input parameters for airport tools, and the generation of contours around airports. The flightpath data holds all the geometry/distance information with respect to stationary observer locations on the ground, whereas NPD curves carry the noise source characteristics information. Due to the complexity and cost involved in the generation of experimental NPD curves, the actual source characteristics captured within the curves is limited to the Sound Power Level (PWL) emitted by the source (aircraft). Therefore, NPDs provide the relationship between the PWL of a given aircraft at a reference flight speed and atmosphere, and the slant distance from the flightpath at a number of engine power settings.

As a result, important information about the characteristics of the source are lost. The most evident example is that of the source directivity. As the flyover occurs the observer (experimental microphone, sitting at a location directly under the flightpath) experiences noise emitted at a constant azimuthal angle 1, therefore all noise emitted by the source at other azimuthal angles in neglected in the generation of NPD curves. Figure 2 illustrates a typical experimental flyover test setup.

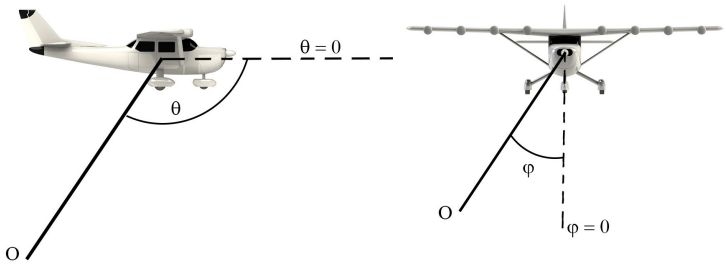

Fig. 1 Polar and azimuthal angles defining observer location. Adapted from [10]

To manage this issue, airport noise models introduce a series of source related correction factors. The contribution therefore, from one flightpath segment to the single event sound exposure level at any observation point is calculated as follows:

$$L_E = L_E(P, d) + \Delta I(\varphi) - \Lambda(\beta, l) \tag{1}$$

where $L_E(P, d)$ is the sound exposure level of due to an aircraft of power setting P at a slant distance of d emitting $L_w(P)$ (PWL, input interpolated from NPD database). The correction factors $\Delta I(\varphi)$ and $\Lambda(\beta, l)$ correspond to engine installation effects (varies depending on the propulsion systems and the mounting location of said system) and the Lateral attenuation (which is a function of the lateral directivity of the source) adjustments respectively. Both correction factors are given in terms of emission angles 1 and are usually modeled by empirical or semi-empirical methods [11],[12].

To accompany these source related corrections, other single event correction terms are applied to account for difference in aircraft speed, sound propagation (atmospheric and ground effects) and finite segments to name a few. Information and exact modelling procedures of the high-fidelity grid-point airport noise model may be found in ECAC Doc 29[2], where the standardised procedures of flightpath discretisation, grid generation and noise data extrapolation is explained in full detail.

B. Noise Surface Method

In this section some key definitions regarding the modeling techniques used within RANE and now RANE v2 will be given; parallels will be drawn between the existing high fidelity tools and RANE v2 but deeper explanations will be given to the features and methodologies that differentiate the two types of models.

As do the high-fidelity models, the noise surface method assumes an aircraft (or generally any airborne vehicle) flying along an infinitely long flight path. The aircraft flies at fixed altitude and engine power setting j, at a constant velocity. As a noise source, the aircraft is treated as a single (lumped) directional source. This therefore allows the source to be totally defined using an acoustic sound power, W (or a Sound Power Level (PWL), L_w) a measure of the total energy radiated by the source as acoustic sound waves; and a directivity factor (the directivity factor may later be seen as directivity function as analytical functions will be used to describe the complex emission patterns). The directivity

factor is responsible of distributing the total amount of acoustic energy into different directions in three-dimensional space, allowing for aircraft to have different acoustical properties in the polar and azimuthal directions 1.

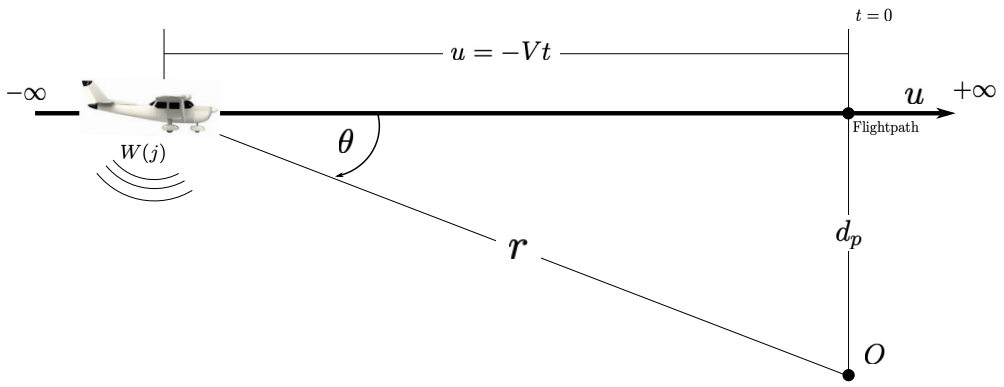

Fig. 2 Diagram of typical flyover procedure for obtaining NPD data.

RANE [7] and Stewart and Carson (1979)[9], worked around the assumption of an isotropic noise source. This results in constant noise Sound Exposure Level (SEL) surfaces in the shape of cylinders to be formed around the infinitely long flightpath. At this point it will be useful to define the SEL noise metric and to distinguish it from other instantaneous noise metrics, as the metric its self is key to the definition and derivation of the noise surfaces. The SEL is a continuous steady level, which over the period of $1s$ contains equivalent total acoustic energy as the actual fluctuating (instantaneous) noise. Mathematically it can be calculated by integrating the instantaneous SPL, $L_P(t)$ (time history) as the aircraft performs the flyover. That is,

$$SEL = 10 \log \int_{-\infty}^{+\infty} 10^{\frac{L_P(t)}{10}} \, \mathrm{d}t \tag{2}$$

The SEL calculated using Equation 2 is for a stationary observer on the ground as the aircraft flies directly overhead. The altitude of the flyover also corresponds to the shortest distance between the observer and the flightpath, this is called the slant distance d_p. For an omnidirectional source, if now we calculate the SEL at all observer locations around the flightpath which have a slant distance equal to d_p of the first location, the resulting SEL would be the same at all observer locations (as the source radiates the same noise in every direction and the infinitely long flightpath does not change from observer to observer). The locations in three-dimensional space of these observers define a 3D surface (or 3D contour), and as is obvious for a omnidirectional source this surface takes the shape of a cylinder. Therefore we define as constant SEL noise surfaces the observer locations around the flightpath that experience the same constant SEL as a result of an aircraft flying along an infinitely long straight flightpath. When talking in terms of Noise Surfaces the slant distance (shortest distance of any particular observer to the flightpath) takes the name Noise Radius, R. For a directional sources, the Noise Radius of the observer locations will not be constant for a constant SEL Noise surface. In order to better understand the concept of constant noise-level surfaces and the radius R that they occur at, we must follow the procedure of calculating the Sound Exposure metric and its assumptions. This procedure is detailed in Section IV.

In order to model a typical 3D aircraft trajectory, discretisation of the smooth continuous flightpath is performed, resulting in flightpath segments. The discretisation is done in such a way that driving flight parameters remain constant along each of the segments. Depending on these flight parameters and noise characteristics of the source, Noise Surfaces of the required dB SEL are fitted around each segment. As a result noise contours on the ground are calculated as the intersection of the 3D Noise surfaces with the ground plane. It is worth reminding that, that similarly with SEL noise surfaces, a Noise Contour is defined as a line of constant value of sound exposure level (dB) around an airport. The noise contour will be composed of contribution due to each of the various segments, and the various pieces of the contour must be determined and suitably pieced together so as to generate the complete contour.

IV. Analytical Principles for directive source contour calculation

A. Noise Surfaces

Using Figure 2 as a reference, let us assume that a test aircraft flies at a fixed altitude and engine power setting j, generating sound power $W(j)$ or Sound-Power-Level (PWL) $L_W(j)$. The resulting noise is measured at a location directly under the flightpath, denoted O, and hence the slant distance d_p, equals the altitude. At this point let us define a cylindrical coordinate system (u, φ, d_p) in which the reference axis u is aligned to the flightpath (Figure 2). This allows observer locations to be defined anywhere in three-dimensional space.

As the aircraft flies along this constant altitude flightpath its position with respect to the observer can be defined using the polar directivity angle θ and the slant distance alone. Therefore we can define the instantaneous Sound Pressure Level observed at position O in terms of the acoustic sound power and the distance between the observer and the aircraft (source) at this point in time, r. It can be seen quite trivially that r is a function of θ and can be written as, $\sin\theta = d_p/r$. Therefore we have:

$$L_p(\theta, \varphi, r) = 10 \log \left[\frac{WD(\theta, \varphi)}{r^2(\theta)} C \right] \tag{3}$$

An additional parameter $D(\theta, \varphi)$, has been introduced. The directivity factor as is called, is defined as the ratio of the sound intensity in the direction (θ, φ) and the mean intensity, $D(\theta, \varphi) = I(\theta, \varphi)/\bar{I}$. For the case of an omnidirectional source the Directivity factor equals 1. C is a constant dependent on the reference pressure $p_{\text{ref}} = 20Pa$ which represents the threshold of human hearing, $C = \rho c/(4\pi p_{\text{ref}}^2)$. As the noise surfaces we are interested in are essentially 3D contours of constant sound exposure levels, we can now define the SEL metric.

Substituting Equation 3 into 2 and performing the following algebraic manipulations we have,

$$\begin{aligned} L_E &= 10 \log \left(\int_{-\infty}^{+\infty} 10^{\frac{L_p(t)}{10}} \mathrm{d}t \right) \\ &= 10 \log \int_{-\infty}^{+\infty} \frac{W(j) D(\theta, \varphi)}{r^2} C \, \mathrm{d}t \end{aligned} \tag{4}$$

From Figure 2, we introduce the substitution:

$$r^2 = d_p^2 + q^2 = d_p^2 + (-Vt)^2 \tag{5}$$

We can now perform the change in integration variable from t to θ,

$$\begin{aligned} q &= -Vt = \frac{d_p}{\tan\theta} \\ t &= -\frac{d_p}{V \tan\theta} \end{aligned} \tag{6}$$

$$\frac{dt}{d\theta} = \frac{d_p}{V \sin^2\theta} \tag{7}$$

Therefore the sound exposure level at the observer from the flyover in the time interval between $[-\infty, +\infty]$ can be expressed as:

$$
\begin{aligned}
L_E &= 10\log\int_{-\infty}^{+\infty}\frac{W(j)D(\theta,\varphi)}{d_p^2+(-Vt)^2}C\,\mathrm{d}t \\
&= 10\log\int_0^{\pi}\frac{W(j)D(\theta,\varphi)C}{d_p^2+(d_p/\tan\theta)^2}\frac{d_p}{V\sin^2\theta}\,\mathrm{d}\theta \\
&= 10\log\int_0^{\pi}\frac{W(j)CD(\theta,\varphi)}{d_p(1+1/\tan^2\theta)V\sin^2\theta}\,\mathrm{d}\theta \\
&= 10\log\frac{W(j)C}{Vd_p}\int_0^{\pi}D(\theta,\varphi)\,\mathrm{d}\theta
\end{aligned}
\tag{8}
$$

Totally anisotropic Source, $D(\theta,\varphi)$: We introduce a variation of the noise emission in the azimuthal direction φ, as well as the polar one. This is the definition of a three-dimensional source. The SEL at any observer O in space can be obtained by the expression in Equation 8. Independently of the dependence of D on the polar angle θ, as the single definite integral is evaluated with respect to θ, the azimuthal angle φ may be treated as a constant. Therefore we essentially get an anti-derivative function $DF(\theta,\phi)$ for which,

$$
\frac{\partial DF(\theta,\varphi)}{\partial\theta} = D(\theta,\varphi) \tag{9}
$$

and the integral can then be evaluated as,

$$
\begin{aligned}
\int_0^{\pi}D(\theta,\varphi)\,\mathrm{d}\theta &= \Big[DF(\pi,\varphi)-DF(0,\varphi)\Big]_0^{\pi} \\
&= f(\varphi)
\end{aligned}
\tag{10}
$$

Substituting this into 8, and using the Noise Radius nomenclature instead of the slant distance,

$$
L_E = 10\log\frac{W(j)C}{VR}f(\varphi) \tag{11}
$$

This indicates that for an directional source, the SEL at any observer location is a function of the azimuthal position of that observer with respect to the flightpath. The polar dependence has been eliminated, though the integration. This expression 11 also serves as the definition of the Noise Surface itself.

To prove this, we begin by using the definition of the Cartesian flightpath coordinate system (u,v,w). The u axis (flight axis) of this coordinate system is aligned with the longitudinal axis of the cylindrical coordinate system (R,φ,u) previously used. The correspondence between the two systems is,

$$
u = u \tag{12}
$$

$$
v = R\cos\varphi \tag{13}
$$

$$
w = R\sin\varphi \tag{14}
$$

with

$$
\begin{aligned}
R &= \sqrt{v^2+w^2} \\
&\implies R^2 = v^2+w^2
\end{aligned}
\tag{15}
$$

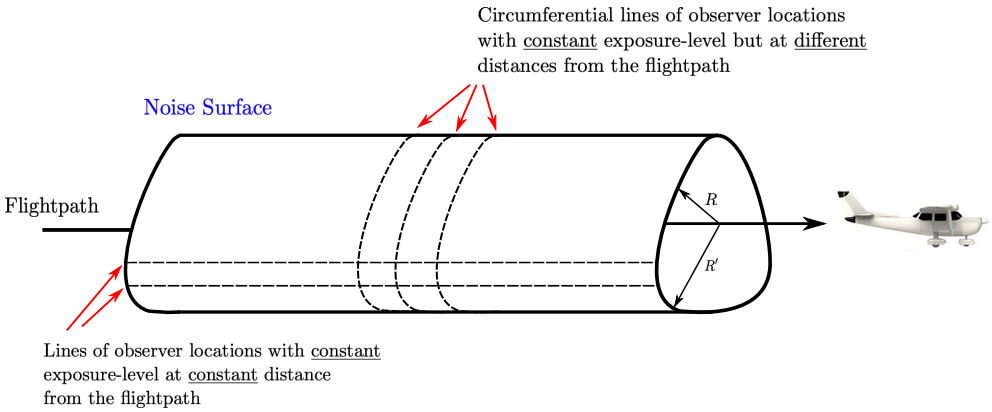

Fig. 3 The noise surface of an azimuthaly directional noise source. The cross section of the surface is no longer a circle, therefore constant exposure levels do not always occur at the same minimum distance from the flightpath.

Using Equation 11 and solving for R, we have,

$$\begin{aligned} L_E &= 10\log\left[\frac{W(j)C}{VR}f(\varphi)\right] \\ 10^{\frac{L_E}{10}} &= \frac{W(j)C}{VR}f(\varphi) \\ R &= \frac{W(j)C}{V10^{\frac{L_E}{10}}}f(\varphi) \end{aligned} \tag{16}$$

Using the conversion from cylindrical coordinates to Cartesian,

$$v^2 + w^2 = \frac{W(j)C}{V10^{\frac{L_E}{10}}}f(\varphi) \tag{17}$$

The right-hand-side of Equation 17 is a function of azimuthal angle (observer lateral position), the equation is similar to that of a cylinder with central axis coincident with the flightpath with the major difference that the radius is not constant,

$$v^2 + w^2 = R_{iso}^2 D_\Lambda(\varphi) \tag{18}$$

R_{iso} represents the Noise Radius of an isotropic source of equal sound power, traveling speed and dB SEL contour requirement. As in RANE the R_{iso} is calculated using NPD databases using the power setting P, aircraft speed V and required SEL contour dB. As will be discussed later in this paper, $D_\Lambda(\varphi)$, the function responsible for the azimuthal radiation of the source can inputted in various forms, analytical and numerical forms. Section V explores the use of Spherical Harmonics as directivity functions. Spherical harmonics prove to be an interesting way of representing a three-dimensional directive source due their analytical properties (expansion capabilities and others) and ease of coefficient interpolation from numerical data or measurements.

Finally, a much more an elegant way of representing the Noise Surface would be in matrix form, as this will make translations and rotations of the surfaces much more straight forward.

$$\mathbf{U}^T\mathbf{S}\mathbf{U} = R^2 D_\Lambda(\varphi) \tag{19}$$

where $\mathbf{U} = (u\ v\ w)^T$ is the position vector and the orthogonal matrix,

$$\mathbf{S} = \begin{bmatrix} 0 & 0 & 0 \\ 0 & 1 & 0 \\ 0 & 0 & 1 \end{bmatrix} \tag{20}$$

The term $D_\Lambda(\varphi)$ can also be converted to the orthogonal (u, v, w) system by using Equations 12 to 14, giving $\mathbf{U}^T\mathbf{S}\mathbf{U} = R^2 D_\Lambda(u, v, w)$.

This result can be interpreted in a couple ways:

- All observer positions whose position is defined by the same azimuthal angle will experience the same exposure level.
- The distance from the flightpath at which the same constant exposure level is now not equal to the slant distance R_{SL} for all observers, but it depends on the azimuthal position and therefore the result of the integration, $f(\varphi)$ in Equation 11.

These two points help illustrate the point that the noise surface does not take the shape of cylinder with a circular cross-section anymore. Rather that of a cylinder with a cross section that depends on the azimuthal (or lateral) directivity of the source. It is worth reminding that the noise surfaces represent observer locations in space, at which the SEL has the same value (essentially three-dimensional contours). The differentiating factor between an isotropic and anisotropic is that these locations do not all occur at the same distance from the flightpath. Instead, the distance depends on the lateral (azimuthal) position of the observers or from a source point of view the lateral directivity of acoustic power emission.

B. Airport model

A typical three-dimensional trajectory consists of a finite amount of straight line segments. Way-points are positioned at the extremities of each of these line segments. Way-point 1 is the start of the take-off roll located at the origin of our (X, Y, Z) airport coordinate system; way-point 2 is lift-off and the general k^{th} segment is between the k^{th} and $(k + 1)$ way-points.

Each segment is characterised by the following:

1) an angle ψ measured positive counter clockwise from the airport X axis to the segment.
2) an inclination angle γ measured positive above the horizontal $X - Z$ plane.
3) a segment length s.
4) a distance R from the aircraft corresponding to the desired Sound Exposure Level (SEL) noise contour and specified power setting.
5) a directivity function $D(\theta, \varphi)$ describing the sources directional radiation properties along that segment

Each k^{th} flightpath segment is aligned with the u axis of the previously defined orthogonal coordinate system (u, v, w). Let us also define an orthogonal coordinate system (x, y, z), in which for each k flightpath segment x is the projection of the u axis on the ground horizontal plane, and the y axis is coincident with the v axis (rotation around the y axis).

As the Noise surface is defined in the (u, v, w) coordinate system is must also be projected to the system defined by position vector $\mathbf{X} = (x\ y\ z)^T$. The transformation between the two vectors $\mathbf{U}$ and $\mathbf{X}$ is,

$$\mathbf{X} = \Lambda_y \mathbf{U} \tag{21}$$

where Λ_y is an orthogonal matrix given by,

$$\Lambda_y = \begin{bmatrix} \cos\gamma & 0 & -\sin\gamma \\ 0 & 1 & 0 \\ \sin\gamma & 0 & \cos\gamma \end{bmatrix} \tag{22}$$

Thus we transform Equation 19, which defines our noise surface, using Equation 21, which gives,

$$\mathbf{X}^T \Lambda_y \mathbf{S} \Lambda_y^T \mathbf{X} = R_{iso}^2 D_\Lambda(x, y, z) \tag{23}$$

where $D_\Lambda(x, y, z)$ is the transformed version of the directivity function.

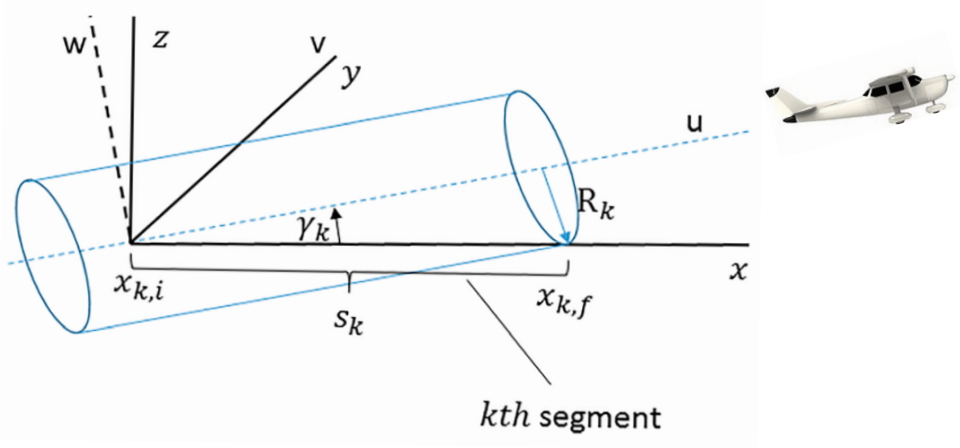

Fig. 4 Definition of the flightpath Cartesian and cylindrical coordinate systems for each segment k, with respect to the orthogonal projection system (x, y, z)

The 2D noise contour is then determined by the intersection of the three-dimensional noise surface in terms of the coordinate system $(x\ y\ x)$ with the ground horizontal plane, $X = (x\ y\ 0)$. The final contour is stitched together on to the airport coordinate system ground plane (X, Y) taking into account the contributions of each of the n^{th} segments using a series of transnational and rotational transforms for each of them. This process is almost identical to RANE [7] therefore it will not be reproduced here.

V. Modeling Source directivity function using Spherical Harmonics

In order to try and use the previous derivations to generate noise contours on the ground for anisotropic noise sources, we need a directivity function that describes the source behaviour. An interesting way to do this is to use spherical harmonics. Their useful analytical properties and ability to decompose any function defined on a sphere in a sum of spherical harmonics allows for multiple ways of testing and verifying the model. Previous studies [13][14][15],that used spherical harmonics to define a three dimensional source proved effective, although the implementation does differ slightly to the one presented here.

Spherical Harmonics are special functions defined on the surface of a sphere. They form a complete set of orthogonal functions and thus an orthonormal basis. Every function defined on the surface of a sphere can be written as sum of these spherical harmonics. As our directivity function is a two-dimensional surface in three-dimensional space, spherical harmonics are appropriate to describe it.

We define the complex sound emission in the direction defined by the two angles θ and ϕ using a decomposition into contributions of spherical harmonics:

$$D(\theta, \varphi) = \frac{1}{N} \left| \sum_{\ell=0}^{n} \sum_{m=0}^{\ell} A_\ell^m Y_\ell^m(\theta, \varphi) \right|^2 \tag{24}$$

The directivity function, $D(\theta, \varphi)$ is given in terms of different contributions of Spherical Harmonics Y_ℓ^m and coefficients A_ℓ^m describing the magnitude of contribution of each harmonic. Using the conventional notation, spherical harmonics are defined on a spherical coordinate system, with angles θ, φ representing the colatitude and longitude, respectively. The colatitude θ, is defined from 0 on the flightpath in front of the aircraft to π on the flightpath behind the aircraft $(0 \leq \theta \leq \pi)$, whereas the longitude φ or azimuth may assume all values $(0 \leq \varphi \leq 2\pi)$ around the flightpath (same convention as used to define observer locations in Figure 1).

As we have introduced an orthogonal flightpath coordinate system (u, v, w), the spherical harmonics coordinate system (θ, φ) is related to it by,

$$\varphi = \arctan\left(\frac{v}{u}\right) \tag{25}$$

$$\theta = \arccos\left(\frac{w}{\sqrt{u^2 + v^2 + w^2}}\right) \tag{26}$$

or reversely,

$$u = \sin\theta\cos\varphi \tag{27}$$

$$v = \sin\theta\sin\varphi \tag{28}$$

$$w = \cos\theta \tag{29}$$

Now the directivity function has been defined in the two useful coordinate systems we can further refine it to fit our purpose. As mentioned, the directivity function is a ratio of the sound intensity in the direction (θ, φ) and the mean intensity. Therefore to retain this property we must ensure the $D(\theta, \varphi)$ is normalised in a way, so the overall acoustic power emitted is unaffected. This condition is satisfied if the integration over the entire spherical surface surrounding the source returns the power of the source,

$$\int_S \frac{WD_s}{4\pi}\,\mathrm{d}S = W(j) \tag{30}$$

or in terms of the directivity function, $D(\theta, \varphi)$,

$$\int_S |D(\theta, \varphi)|^2\,\mathrm{d}S = 1 \tag{31}$$

We take the square of the magnitude as we are dealing with intensity ratios rather than pressure ratios. The normalisation factor N ensures that this condition is satisfied.

We have now fully defined our directivity function in terms of spherical harmonics. In order to calculate the noise-surface and therefore noise contours on the ground of such a source, we need to follow the flyover procedure described previously and calculate the exposure levels at different observer locations. This will define the noise surface of the anisotropic source.

$$\begin{aligned} L_E &= 10\log\frac{W(j)C}{VR}\int_0^\pi D(\theta,\varphi)d\theta \\ &= 10\log\frac{W(j)C}{NVR}\int_0^\pi \left|\sum_{\ell=0}^{n}\sum_{m=0}^{\ell} A_\ell^m Y_\ell^m(\theta,\varphi)\right|^2 d\theta \end{aligned} \tag{32}$$

But, as spherical harmonics are complex functions we have,

$$\left|\sum_{\ell=0}^{n}\sum_{m=0}^{\ell} A_\ell^m Y_\ell^m(\theta,\varphi)\right|^2 = \left(\sum_{\ell=0}^{n}\sum_{m=0}^{\ell} A_\ell^m Y_\ell^m(\theta,\varphi)\right)\left(\sum_{\ell=0}^{n}\sum_{m=0}^{\ell} A_\ell^m Y_\ell^m(\theta,\varphi)\right)^* \tag{33}$$

In order to demonstrate the analytical calculation of the integral in Equation 32, the spherical harmonic expansion has to be truncated, to limit the amount the amount of terms in the product of the complex sum times its conjugate in Equation 33. Therefore we limit the degree ℓ of the spherical harmonic expansion to just 1, this means for this specific demonstration the directivity function will be built of combinations of a monopole the three different dipoles. So,

$$\left(\sum_{\ell=0}^{1}\sum_{m=-1}^{\ell} A_\ell^m Y_\ell^m(\theta,\varphi)\right)\left(\sum_{\ell=0}^{1}\sum_{m=-1}^{\ell} A_\ell^m Y_\ell^m(\theta,\varphi)\right)^* =$$

$$= (A_0^0Y_0^0 + A_1^{-1}Y_1^{-1} + A_1^0Y_1^0 + A_1^1Y_1^1)(A_0^0Y_0^0 + A_1^{-1}Y_1^{-1} + A_1^0Y_1^0 + A_1^1Y_1^1)^*$$

$$= A_0^0Y_0^0(A_0^0Y_0^0)^* + A_0^0Y_0^0(A_1^{-1}Y_1^{-1})^* + A_0^0Y_0^0(A_1^0Y_1^0)^* + A_0^0Y_0^0(A_1^1Y_1^1)^*$$

$$+ A_1^{-1}Y_1^{-1}(A_0^0Y_0^0)^* + A_1^{-1}Y_1^{-1}(A_1^{-1}Y_1^{-1})^* + A_1^{-1}Y_1^{-1}(A_1^0Y_1^0)^* + A_1^{-1}Y_1^{-1}(A_1^1Y_1^1)^* \tag{34}$$

$$+ A_1^0Y_1^0(A_0^0Y_0^0)^* + A_1^0Y_1^0(A_1^{-1}Y_1^{-1})^* + A_1^0Y_1^0(A_1^0Y_1^0)^* + A_1^0Y_1^0(A_1^1Y_1^1)^*$$

$$+ A_1^1Y_1^1(A_0^0Y_0^0)^* + A_1^1Y_1^1(A_1^{-1}Y_1^{-1})^* + A_1^1Y_1^1(A_1^0Y_1^0)^* + A_1^1Y_1^1(A_1^1Y_1^1)^*$$

Substituting Equation 34 in the integral of Equation 32, the calculation can be broken down into the sum of much simpler integrals, the first integral for example:

$$\int_0^\pi A_0^0Y_0^0(A_0^0Y_0^0)^*\,\mathrm{d}\theta \tag{35}$$

All 16 of these integrals are similar and their calculation follows the same procedure. For demonstration, three of these integrals will be analytical calculated here. For the rest, only the final result will be shown.

To begin, we look at the definition of spherical harmonics. Spherical harmonic are the angular solutions to Laplace's equation in spherical coordinates. They are essentially trigonometric functions which can be represented as a complex exponential, and associated Legendre polynomials as follows,

$$Y_\ell^m = N_\ell^m e^{im\varphi} P_\ell^m(\cos\theta) \tag{36}$$

as mentioned, ℓ represents the degree of the spherical harmonic and m the order. P_ℓ^m are the associated Legendre polynomials, while N_ℓ^m is a normalisation factor.

Legendre polynomials $P_\ell^m(x)$ are the canonical solutions of the general Legendre equation. By re-parameterising in terms of angles, by letting $x = \cos\theta$ we get the more useful form of the functions that also appears in the Spherical Harmonic definition above. The first few polynomials, parameterised this way can be seen bellow,

$$P_0^0(\cos\theta) = 1$$

$$P_0^1(\cos\theta) = \cos\theta \tag{37}$$

$$P_1^1(\cos\theta) = -\sin\theta$$

Also to include the term for negative values of m, we can use the following expression,

$$P_1^{-1}(x) = -\frac{1}{2}P_1^{-1}(x) \tag{38}$$

Expressions 36 to 38 allow for the integrals to be simplified into integrals involving combinations of trigonometric functions that can easily be evaluated using techniques such integration by parts.

1st Integral: The first integral to evaluate is a diagonal term,

$$
\begin{aligned}
&\int_0^{\pi} A_0^0 Y_0^0 (A_0^0 Y_0^0)^* \,\mathrm{d}\theta = \\
&= \int_0^{\pi} A_0^0 (N_0^0 e^{i.0.\varphi} P_0^0(\cos\theta)) A_0^0 (N_0^0 e^{-i.0.\varphi} P_0^0(\cos\theta)) \,\mathrm{d}\theta \\
&= \int_0^{\pi} (A_0^0)^2 (N_0^0)^2 e^{i.0.\varphi} e^{-i.0.\varphi} (P_0^0(\cos\theta))^2 \,\mathrm{d}\theta \\
&= (A_0^0)^2 (N_0^0)^2 \int_0^{\pi} (P_0^0(\cos\theta))^2 \,\mathrm{d}\theta \\
&= (A_0^0)^2 (N_0^0)^2 \int_0^{\pi} \mathrm{d}\theta \\
&= \pi (A_0^0)^2 (N_0^0)^2
\end{aligned}
\tag{39}
$$

2nd Integral:

$$
\begin{aligned}
&\int_0^{\pi} A_0^0 Y_0^0 (A_1^{-1} Y_1^{-1})^* \,\mathrm{d}\theta = \\
&= \int_0^{\pi} A_0^0 (N_0^0 e^{i.0.\varphi} P_0^0(\cos\theta)) A_1^{-1} (N_1^{-1} e^{-i.(-1).\varphi} P_1^{-1}(\cos\theta)) \,\mathrm{d}\theta \\
&= \int_0^{\pi} A_0^0 A_1^{-1} N_0^0 N_1^{-1} e^{i\varphi} P_1^{-1}(\cos\theta) \,\mathrm{d}\theta \\
&= A_0^0 A_1^{-1} N_0^0 N_1^{-1} e^{i\varphi} \int_0^{\pi} (-\frac{1}{2} P_1^1(\cos\theta)) \,\mathrm{d}\theta \\
&= \frac{1}{2} A_0^0 A_1^{-1} N_0^0 N_1^{-1} e^{i\varphi} \int_0^{\pi} \sin\theta \,\mathrm{d}\theta \\
&= A_0^0 A_1^{-1} N_0^0 N_1^{-1} e^{i\varphi}
\end{aligned}
\tag{40}
$$

3rd Integral:

$$
\begin{aligned}
&\int_0^{\pi} A_0^0 Y_0^0 (A_1^{-1} Y_1^{-1})^* \,\mathrm{d}\theta = \\
&= \int_0^{\pi} A_0^0 (N_0^0 e^{i.0.\varphi} P_0^0(\cos\theta)) A_1^{-1} (N_1^{-1} e^{-i.(-1).\varphi} P_1^{-1}(\cos\theta)) \,\mathrm{d}\theta \\
&= \int_0^{\pi} A_0^0 A_1^{-1} N_0^0 N_1^{-1} e^{i\varphi} P_1^{-1}(\cos\theta) \,\mathrm{d}\theta \\
&= A_0^0 A_1^{-1} N_0^0 N_1^{-1} e^{i\varphi} \int_0^{\pi} (-\frac{1}{2} P_1^1(\cos\theta)) \,\mathrm{d}\theta \\
&= \frac{1}{2} A_0^0 A_1^{-1} N_0^0 N_1^{-1} e^{i\varphi} \int_0^{\pi} \sin\theta \,\mathrm{d}\theta \\
&= A_0^0 A_1^{-1} N_0^0 N_1^{-1} e^{i\varphi}
\end{aligned}
\tag{41}
$$

A. Comparison between analytic and numerical integration of Directivity Functions

The calculation of the integral in Equation 8 has been performed numerically, in order to accommodate discretised directivity data, and analytically (using spherical harmonics) as presented in the previous sections. In order to validate the numerical integration, a few examples examples are presented below for different directivity functions using combinations of the monopole and the three different dipoles. The figures compare the value of the following integral , for different $D(\theta, \varphi)$. They are presented in polar plots, with the axial variation being in the variable φ.

$$\int_0^{\pi} D(\theta, \varphi)\, \mathrm{d}\theta \tag{42}$$

Figure 5 presents example calculations using the monopole and dipole to define the directivity functions. The result of the integration along the polar angle θ, is a function in φ, the azimuthal angle. The polar plots show how the function varies with φ. In each case the coefficients of the spherical harmonic expansion are presented in matrix form as, $A_\ell^m = [A_0^0\ A_1^{-1}\ A_1^1\ A_1^0]$ to distinguish between the coefficients of different order and degree.

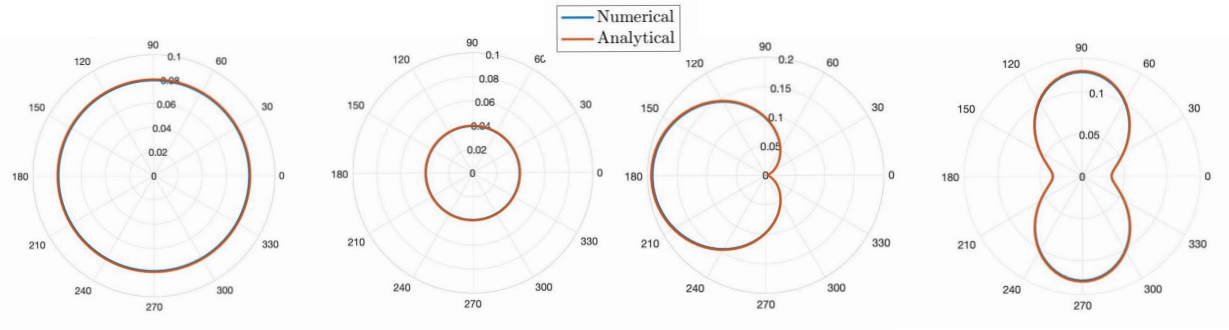

Fig. 5 Comparison of the analytical and numerical calculation of the integral in Equation 32 for four different directivity functions of which the coefficients from left to right are: $A_\ell^m = [1\ 0\ 0\ 0]$**,** $A_\ell^m = [0\ 0\ 0\ 1]$**,** $A_\ell^m = [1\ 1\ 0\ 0]$**,** $A_\ell^m = [1\ 1\ 1\ 1]$**.**

VI. Contour Area and Connections

A. Contour Area

Once the contour coordinates have been found, the area within the contour is calculated using numerical integration. The contour is split into an upper and lower region, and the area of each is calculated using the trapezoidal rule. Then the area of the lower region is simply subtracted form that of the upper to give the area within the required contour.

B. Connections and Extremities

The regions of the contour where the contributions from two different segments meet are of special interest. In many cases (e.g. turns, power setting changes) discontinuity of the contour arises and the transition from one segment to another is not smooth. The lack of predictive ability of model in these regions is due to the segment interaction error discussed in Section VII. The noise at the observer locations in these regions is heavily influenced by both the preceding flightpath segment and the following one.

In order to model these connection regions a simple spline was used, defined by points on the contours of both the segments adjacent to the region. These points, also called control points of the spline, are chosen as points on their respective segments where negligible contribution to noise exposure has occurred from other segments (or sound exposure at these points is predominantly due to the aircraft flying along the segment they belong to). The simple splines used are called Bezier curves. They are parametric curves defined by a set of control points. The first, P_0 and last P_n control points are always the end points of the curve; however, the intermediate control points (if any) generally do not lie on the curve. The number of control points also defines the order of the curve (n = 1 for linear, 2 for quadratic, etc.). Figure 6 shows two example calculations where Bezier curves were used to model the segment connection regions.

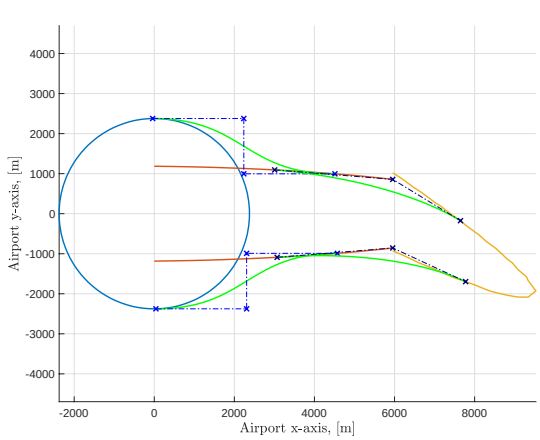

(a) Vertical take-off with turn, 75 dB SEL contour.

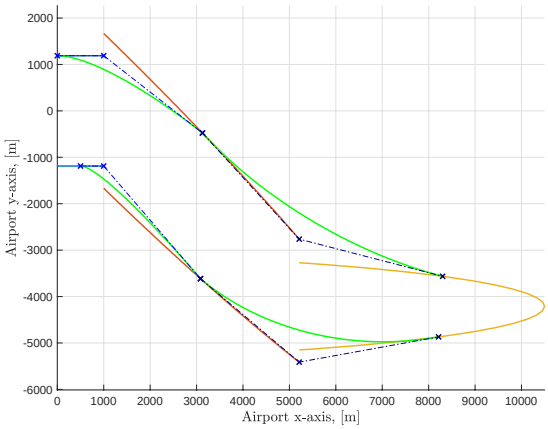

(b) Conventional take-off with two turns, 75 dB SEL contour.

Fig. 6 Modelling of connecting regions through the use of Bezier curves.

For the contour application, the first and last control points are chosen on the contours of the two connecting segments respectively. The order of the curve and therefore the total number of control points is determined by the type of transition between the two segments. It can be seen that in Figure 6 on the left, two types of Bezier curves have been used. The green ones using 4 control points (cubic curve) are modelling the transition from one Noise radius to another. While for a turn transition of the same radius, where the contours mostly match up but a slight miss-alignment occurs, the transition can be modelled using a quadratic (or just three control points) curve, as in the right-hand-side of Figure 6. When a noise radius change occurs, a huge discontinuity in the contour is present (a step type discontinuity). This type of transition requires an extra control point for a smooth contour to be modeled.

To demonstrate the effectiveness of Bezier curves for the modeling of the connecting regions between segments two different examples are presented in Figure 7, both implementing different combinations of transitions. The contours are compared against an in house grid-point method, introduced in the validation Section VII

VII. Validation

To assess the capability of the modifications made to RANE for estimating noise exposure contours and the area within them a multi-step process is required. The validation procedure is broken down into two main sections, identified by the directivity of the source.

The initial benchmarking test that took place was comparing the capability of the modified RANE model to calculate contours and areas of omnidirectional sources. This was achieved using an in house grid-point method. This test was to assess that the original capabilities of RANE were not altered with the addition of non-isotropic sources. To further validate these conclusions, tests will be performed using comparisons against the FAA's AEDT model, a well established tool in the airport noise community.

A. Benchmarking against in-house grid-point method

In this section a simple grid-point method model is described and implemented in order to compare sound exposure level contours with the noise surface method developed. The ground surface or airport coordinate system is defined by a Cartesian coordinate system (x, y, z) with the runway laying in the $x - y$ plane. The origin of the coordinate system is positioned at the start of the ground roll with the runway extending out in the positive x direction. In the case of a vertical take-off the origin is again placed at the point where vertical flight is initiated.

Each individual aircraft movement is described by its three-dimensional flightpath, engine power setting and speed along it. The flightpath is discretised into simple linear segments defined by a waypoint at the start of each segment. The waypoints carry information that describes the operation and movement of the aircraft along the following segment. The flight parameters, as they're called are assumed to remain constant along the length of the segment and are the

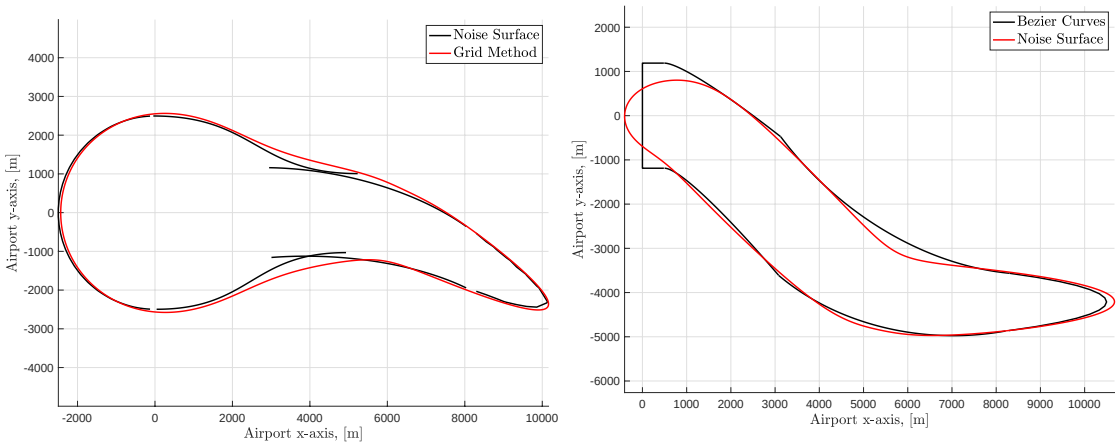

(a) Vertical take-off with turn, 75 dB SEL contour.

(b) Conventional take-off with two turns, 75 dB SEL contour.

Fig. 7 Two different cases of using Bezier curves to approximate segment connections compared to the grid-method (See following Section).

following: (1) an inclination angle, (2) an angle of rotation, (3) the length of the segment, (4) the engine power setting (or in this case, we define the source as an acoustic monopole emitting noise of some SPL value at the reference distance of 1m) and (5) the speed of the aircraft along the segment. These parameters are almost identical to the ones describing the flightpath of the noise surface method, as the flightpath is the same. Each segment is further discretised in to a number of points N_s modelling the movement of the aircraft along this segment.

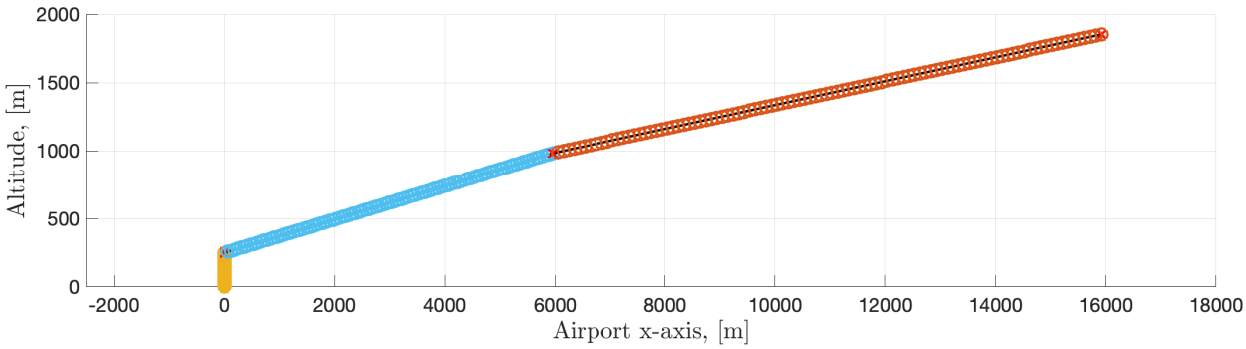

Fig. 8 Discretisation example of flightpath segments for grid-point method.

Using the coordinates of the final point on the last segment of the flightpath an appropriately sized rectangular grid is defined on the ground ($x-y$ plane). Each point on the grid represents an observer location at which the sound exposure levels of the aircraft movement will be calculated. As the aircraft continues to fly even after the end of the final segment, an extension to the final segment is added. The segment is extended until the acoustic contribution (SPL) to all points on the grid drops to zero.

The sound level at each grid point due to the aircraft at any point in time is given by:

$$Lt_{k,i} = L_{p,source} - 20\log\left(r\right) \tag{43}$$

where r is the distance between the specific grid point (observer) and the aircraft at that point in time, and k,i are counters indicating the position of the aircraft along the discretised flightpath. Therefore as the aircraft flies along the discretised flightpath (assuming $t = 0$ occurs when the aircraft is positioned at the origin for at take-off procedure) the Sound exposure level at each individual grid point may be calculated as:

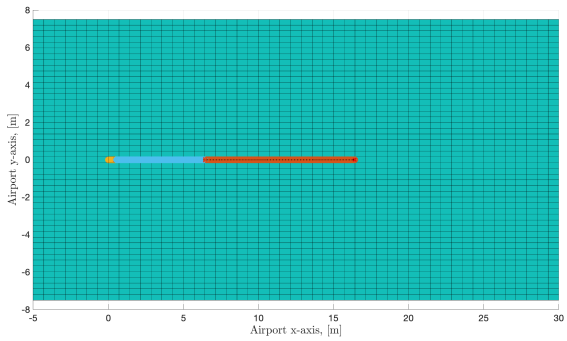

(a) The airport plane (X, Y) grid defined by the flight-path for the calculation of the grid-point method sound exposure contour maps.

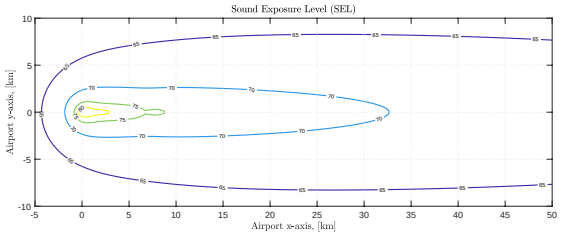

(b) An example contour map calculated using the grid method.

Fig. 9 Grid-method numerical validation model geometry and example contour map.

$$SEL = 10 \log \left(\sum_{k=1}^{K} \sum_{i=1}^{N_s} 10^{\frac{Lt_{k,i}}{10}} \Delta t \right) \tag{44}$$

where K denotes the number of segments including the extension to the last segment. Δt is calculated using the aircraft speed along the segments, along with the segment length and number of discretisation points of the segment, N_s. Once the SEL of the single aircraft movement has been calculated at each of the grid point a contour map can be created. An example airport contour map can be seen in Figure 9.

The contour map is composed of multiple contour lines, ranging (in this example) from 60 to 80 dB SEL. The calculation time is highly dependant on the size of the grid and the number of discretisation points in each dimension. The flightpath discretisation also contributes to significantly to the computation times. This example computation with 1,000,000 grid points and 100 point along each of the flightpath segments took a total time of 238.258 s. Although excessive, this number of grid-points was chosen to ensure convergence; and as grid-method generation and optimisation techniques are out of the scope of this project, this scale of computation times for simple single runway, 3-5 segment flightpaths examples is manageable for running validation test cases. The equivalent Noise Surface example was calculated in 36.194 s, almost 6.6 times faster. (NOTE: these calculations were performed on personal laptop computers). Larger more complex test examples will be tested against FAA's AEDT.

Table 1 Example input parameter table for conventional and vertical take-off procedures of an omnidirectional noise source.

	Conventional			**Vertical**		
	Segment 1	**Segment 2**	**Segment 3**	**Segment 1**	**Segment 2**	**Segment 3**
Inclination angle, γ (deg)	0.5	7.5	5	**90**	7.5	5
Rotation angle, ψ (deg)	0	0	0	0	0	0
Segment length, s (m)	1000	6,000	60,000	**100**	6,000	60,000
Speed, v (m/s)	100	100	100	**1**	100	100
Source SPL, L_p (dB)	120	120	120	120	120	120
Noise radius, R (m)	1,110	1,110	1,110	**2,000**	**1,050**	**1,050**

The following Figures from **??** to **??** showcase example calculations using RANE v2 and comparing to the grid-point method, with Figure **??** illustrating an interesting case of a vertical take-off procedure. The inputs parameters for the case of a simple three segments take-off (Figure **??**) are presented in Table 1. Slight alterations to the inputs are made for the cutback and turn examples. All examples assume an omnidirectional source by setting all Spherical Harmonics

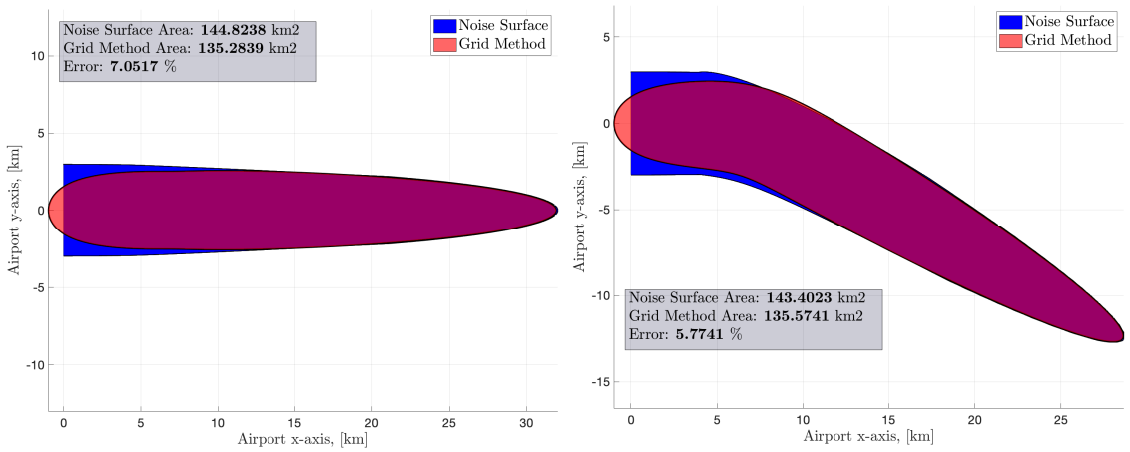

(a) Conventional take-off. **(b) Conventional take-off.**

Fig. 10 The 70 dB SEL contour of an isotropic source. Contour area comparison between RANE v2 and the grid-point method.

coefficient to zero other than the monopole term one. The decision to first test an isotropic source was made due to the fact that, designing an grid-point method with directivity features in also out of the scope of this project. Thus for initial validation isotropic sources were used. As discussed, further validation is taking place against calculations using AEDT. These calculations will be performed for helicopters and their directional nature. Therefore the newly added modification of RANE v2 can be properly verified.

For a given source strength and required sound-level contour, the noise radius input, R for the noise surface method is calculated using the definition of the SEL metric, Equation 2 by performing an artificial flyover.

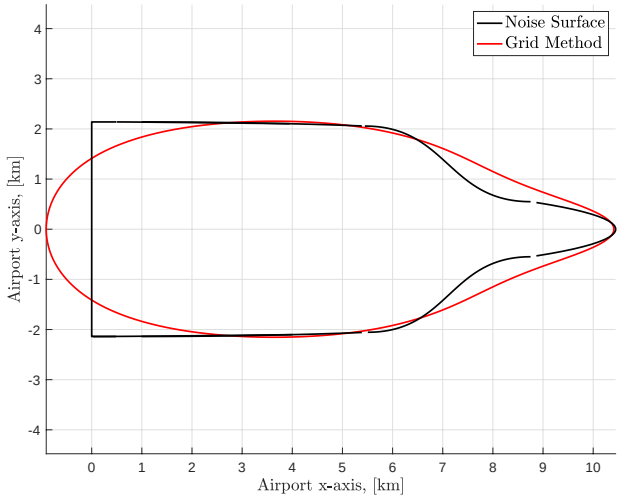

Fig. 11 The 75 dB SEL contour of an isotropic source, conventional Take-off with cutback. Contour area comparison between RANE v2 and the grid-point method.

Table 1 also shows the different inputs required for a vertical take-off compared to a conventional fixed wing flightpath. Interesting parameters have been highlighted in red and green. It is interesting to point out the short vertical segment and the speed along it. These features were modeled after typical flight profiles and operational procedures of helicopters, operating at helipads according to the FAA [16].

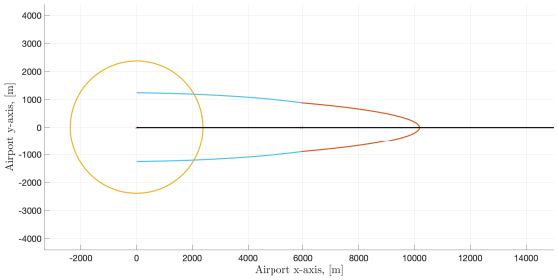

(a) RANE v2 set-up and contour lines with flightpath indicated in black.

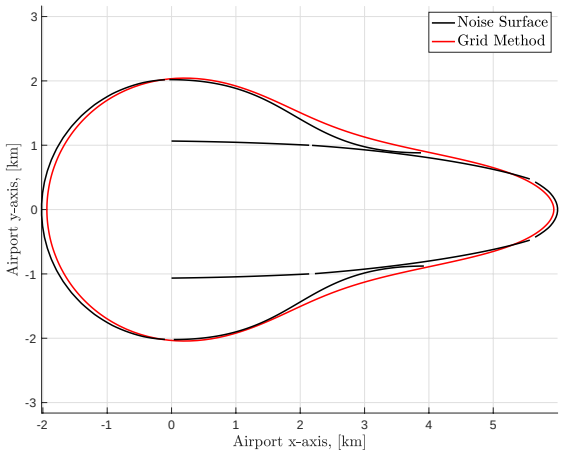

(b) Comparison between RANE v2 and the grid-point method of the 75 dB SEL contour.

Fig. 12 Isotropic source during vertical take-off.

B. Benchmarking against FAA's AEDT

As previously mentioned, AEDT is a comprehensive, grid-point model that operates in a similar manner to the in house grid-point method previously described. It assesses the noise impact of conventional aircraft fleets around airports, in various metrics, typically noise exposure contours around airports. In addition to conventional fixed wing aircraft, AEDT carries capability of assessing helicopter operations around airport and helipads/heliports. The Heliport Noise Model (HNM) module was incorporated into INM (Integrated Noise Model) with a helicopter noise database collected through both FAA and manufacturer certification measurements and later into the current version of AEDT.

In order to compare results to AEDT predictions two types of directivity must be specified. First, the start-of-roll directivity function. For helicopters, this directivity correction in AEDT accounts for static radiation patterns that occurs while the vehicle is on or slowly ascending vertically from the helipad. To account for this, static directivity data was fitted by a sinusoidal curve fitting model and then decomposed into spherical harmonics. The spherical harmonics expansion was then used as an input for the directivity function on the initial segment of the flightpath. Secondly, lateral directivity corrections in AEDT for helicopters are accounted for using 3 NPD curves for every operation, a centre one (directly under the flightpath), a left one ($\varphi = -45°$ with respect to the flightpath) and a right one ($\varphi = 45°$). All levels at azimuthal angles between the left and centre curves are interpolated logarithmically (the same applies for all values of φ between the right and centre). For values of $\varphi > 45°$ and $\varphi < -45°$ the level at the right ($\varphi = 45°$) is taken and for the left respectively. In order to generate a directivity function suitable for RANE v2, the three levels at the sound exposure of interest were used to (similarly with the static directivity case) generate a sinusoidal curve fitting for all values of φ between $-90°$ and $90°$. This fitting was again decomposed in to spherical harmonics and used as input to RANE v2.

Three helicopter models were used in this comparison, to cover three different weight (size) groups. The Schweiser 300C a light utility helicopter, the Eurocopter AS365 Dauphin a medium sized also utility helicopter and the Boeing CH-47 Chinook a large transport helicopter were used. The default helicopter flight profile from AEDT 3c was used along with a default linear flight track. The total flightpath is broken down into 4 major segments: a. A vertical take-off, b. a horizontal acceleration, c. a climb to altitude and d. a horizontal steady level flight. These are also the segments used to model the take-off operation in RANE v2. The resulting contour comparison for all three helicopters may be seen in Figure 15.

Finally, Figure 14 shows a contour map comparison for the Boeing CH-47 Chinook. The map includes sound level of 75 db, 65 dB and 55dB. RANE again matches the AEDT prediction very well, however it is evident that error increases as we look at lower SEL levels.

Overall RANE v2 does a great job of matching the contours generated by AEDT. Slight errors in the static directivity prediction (occurring in the first segment, around the $(0, 0)$ origin of the airport plane) are due to curve fitting errors and the truncation of the spherical harmonic expansion to only $\ell = 12$. Errors associated with the noise surface method its self are described in the following Section.

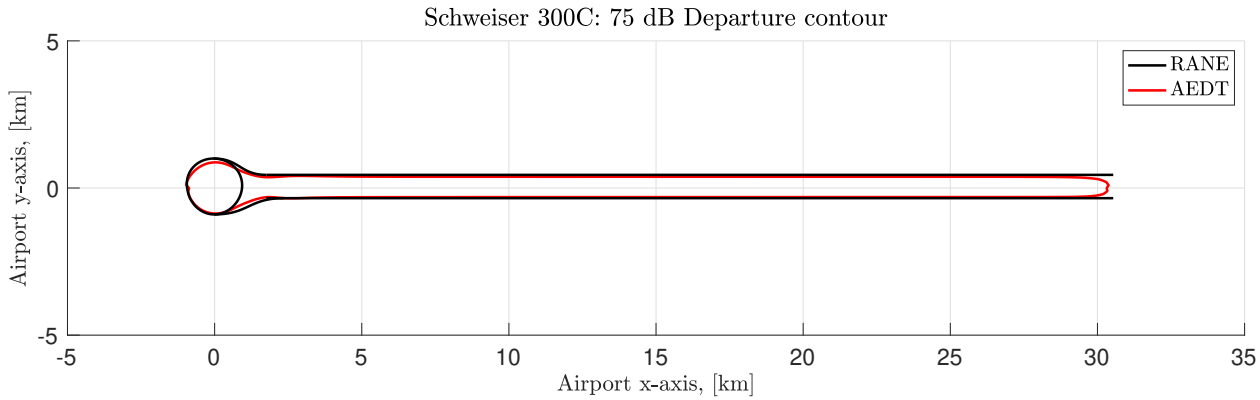

(a) Schweiser 300C

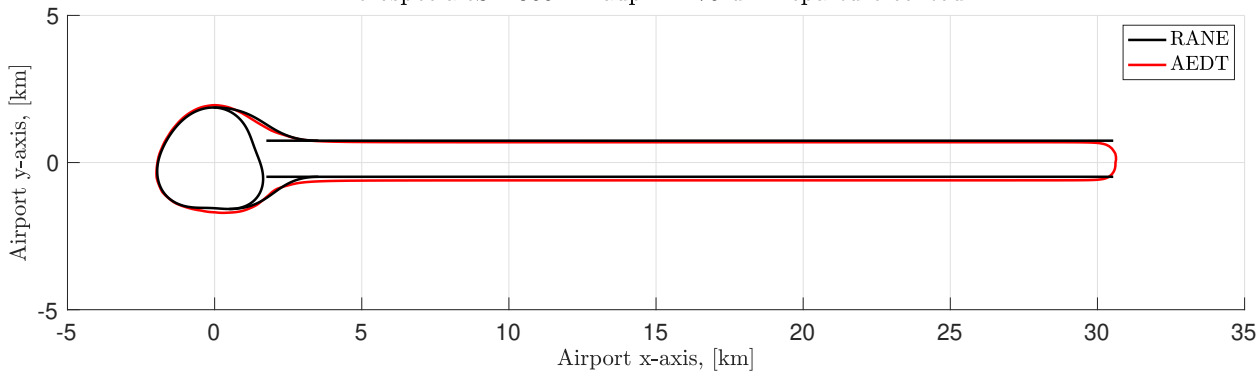

(b) Eurocopter AS365 Dauphin

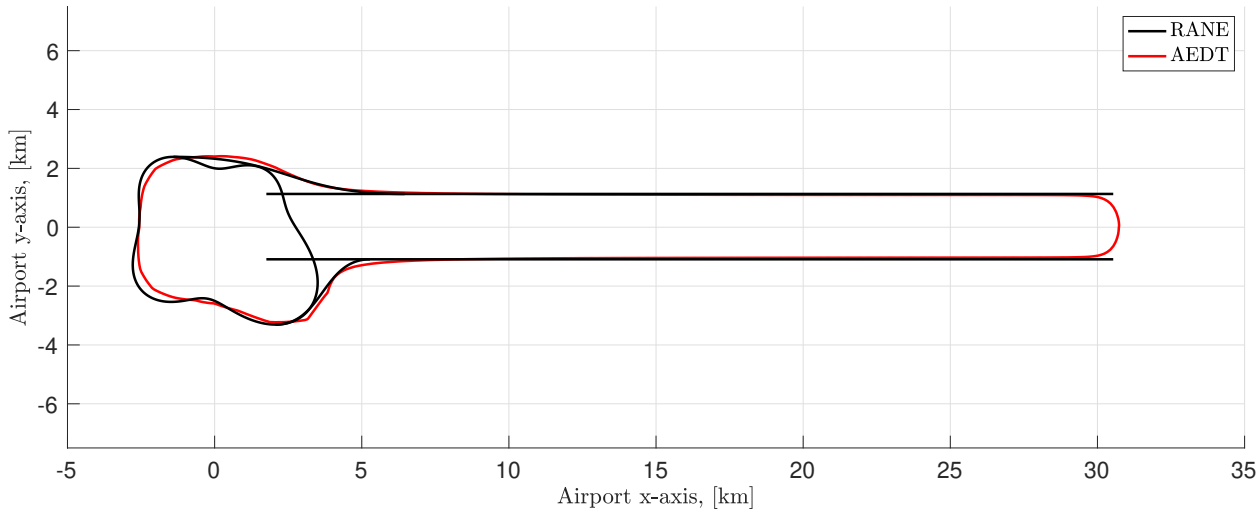

(c) Boeing CH-47 Chinook

Fig. 13 Comparison between the RANE v2 and AEDT 3c prediction for three different helicopters.

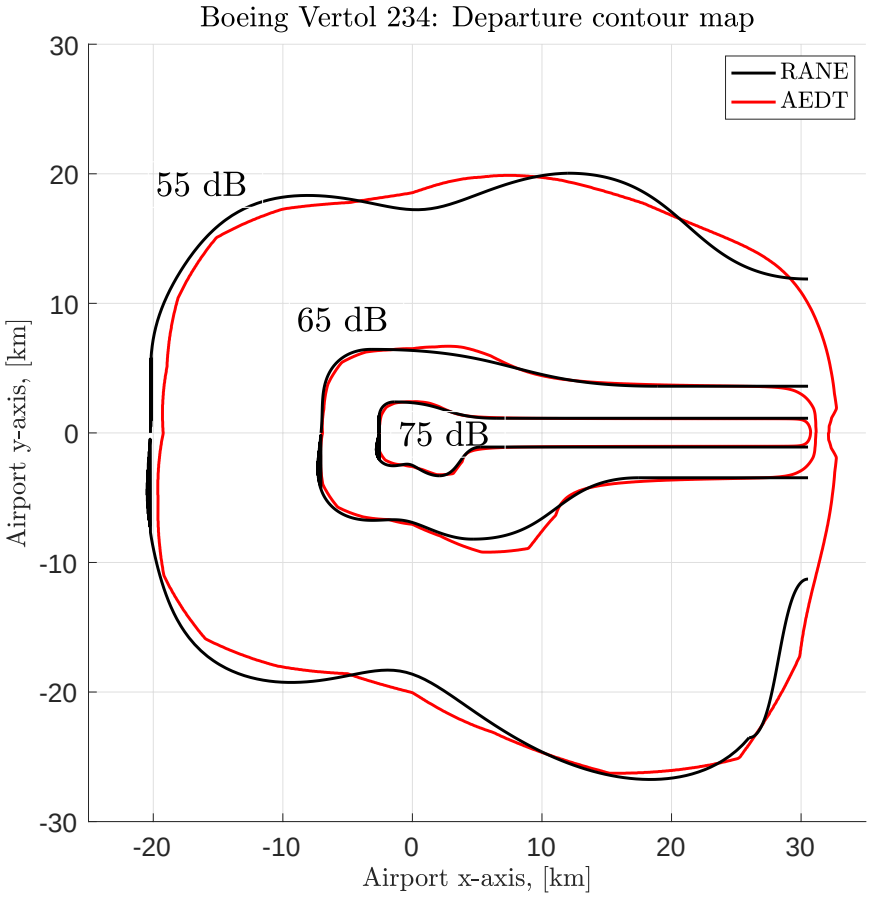

Fig. 14 SEL noise exposure contour map for Boeing CH-47 Chinook. Comparison between AEDT and RANE predictions.

C. Sources of Error

1. Finite Segment Error

As evident, the model of RANE and subsequent update RANE 2, assumes that sound exposure surfaces are formed around the flightpath as the aircraft flies from $-\infty$ to $+\infty$. These surface are then positioned around the segments of a discretised version of the actual flightpath the aircraft takes during take-off and landing operations. As long as these segments are of significant length, where the contribution of the remaining parts of the infinite segment are negligible compared to the actual segment itself, the error in the actual position of the contour, and therefore the noise radius itself should also be negligible. The shorter the discretised segment of the flightpath is, the less of a contribution it has compared to the infinite flyover the noise surface was calculated with.

This error can be dealt with by altering the limits of integration when calculating the directivity function. Instead of assuming the aircraft flies along an infinitely long flightpath, meaning the integration limits in terms of the variable θ are 0 to π; for each segment the aircraft flies flightpath equal to the segment length. This requires that the new limits of integration for the noise surfaces are within the old ones i.e. $0 <$ lower limit and upper limit $< \pi$, therefore the interval is of smaller length.

2. Segment interaction error

An error arises in the calculation of the noise radius for the noise surface method. The noise radius for each individual segment is calculated through the use of NPD curves for a specific power setting, speed and sound exposure level. NPD curves assume a steady level flyover a single observer from effectively $-\infty$ to $+\infty$ for the calculation of the exposure levels. Therefore for any given point on the contour, the noise is due to one segment alone. The contribution

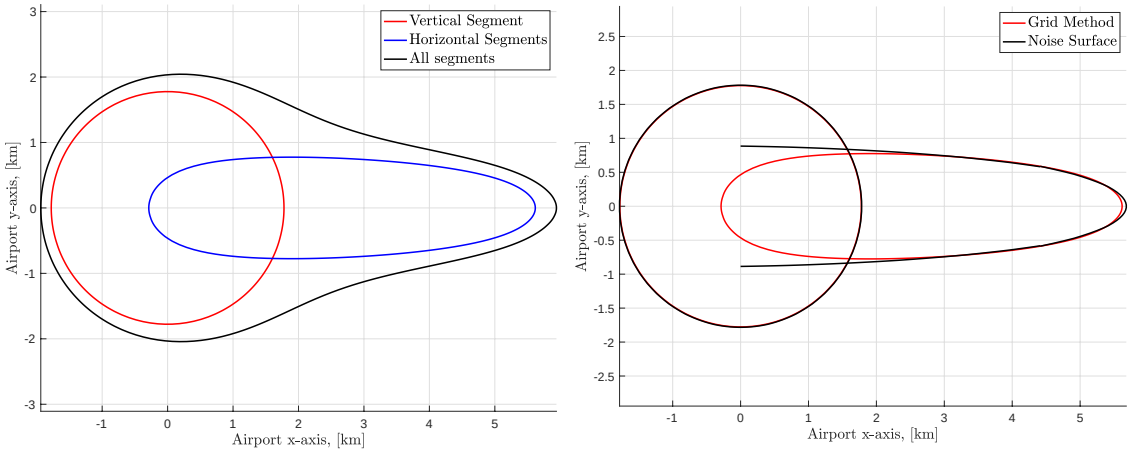

(a) Grid-point method 75 dB SEL contour: Comparison between the vertical and horizontal segment individual calculations and the total flightpath calculation.

(b) Comparison between RANE v2 and the grid-point method when calculating the vertical and horizontal segments individually.

Fig. 15 Demonstration of segment interaction error using results from the grid-method and RANE v2.

of all other segments, to that specific contour is neglected; this causes the noise segment method to under estimate the noise radius, as contributions from other segments would increase noise exposure at these observer locations causing the contour to move further away from the flightpath.

To demonstrate this, two tests were performed. One was using the grid method alone, where a vertical take off operation was modeled in two different ways. (a) All segments of the flightpath contributed to the calculation of the exposure contour maps and (b) the vertical segment of the flightpath was calculated separately than the two horizontal ones. The result can be seen in Figure **??**. The red contour is of significantly larger area, due to the contributions of all segments to the sound exposure level.

To further illustrate the point, the noise surface method calculation for the identical operation is show in Figure **??** against the grid-point method contour where the vertical and horizontal parts have been calculated separately. The match is clearly much better. The error that occurs in the initial vertical segment can be proven to be as a result of the finite segment error discussed previously, due to the fact that the vertical segment is relatively short, and therefore the integration limits of the flyover must be altered to capture the real exposure on such a short segment.

VIII. Conclusion

This paper presents an update to the RANE model for generating noise exposure contours around airports. This update implements a new method for accounting for overall aircraft directivity. Preliminary noise contours are generated through the use of a discretised flightpath and Noise Surfaces. Analytical derivation of the noise surfaces is performed using spherical harmonics as the aircraft directivity function. The developed model is then used to demonstrate the potential noise contours of an omnidirectional (defined using the monopole term from the harmonic expansion) while performing a series of different operations including vertical take-offs. Finally, preliminary comparisons with the AEDT helicopter module for the Bell 206 JetRanger helicopter were performed and showcased, while more detailed and extended comparisons are in the working for validation purposes.

Future Work

Along with complex emission patterns and individual source directivity, UAM vehicles as discussed present novel challenges in terms of operation procedures. Vertical flight and hover capabilities of eVTOL. Transition from vertical to horizontal flight and reverse is a complex operation in terms of aerodynamics, propulsion systems and, therefore, noise. During this transition period, the dominant noise sources may shift, allowing for changes in overall noise power output, and in terms of source directivity.

The framework built within this paper, allows for a source coordinate system to be implemented. Using a tilt-rotor as an example, the wing-rotor subsystem rotates during a transition operation with respect to observers on the ground. This means the dominant dipole like loading and thickness noise components of the propeller noise will also experience a change in axis. This sort of source coordinate system and potential for transition calculations are currently being implemented into RANE v2, with preliminary noise surfaces already being generated. Finally, the capabilities of RANE v2 are also being extended to allow for contour generation due to aircraft fleet, and not just single events. This will allow for studies on the effect of UAM vehicle integration to current aviation systems.

The work presented in this report is part of a larger ongoing project at the University of Southampton. This project will look at novel aircraft in the fixed wing and rotorcraft families, with specific focus on the growing Urban Air Mobility sector. Modeling the different sources on these aircraft along with their highly directive nature ground noise predictions will be made.

References

[1] Goyal, R., "Urban Air Mobility (UAM) Market Study," Tech. rep., National Aeronautics and Space Administration (NASA), November 2018.

[2] "Report on standard method of computing noise contours around civil airports, vol. 2: Technical guide," Tech. rep. ecac.ceac doc. 29, 4th ed, European Civil Aviation Conference (ECAC), December 2005.

[3] Centre, E. E., "Aircraft noise and performance (ANP) database v2.1," , 2016. URL `http://www.aircraftnoisemodel.org`.

[4] Koopmann, J., Hansen, A., Hwang, S., Ahearn, M., and Solman, G., "The CAA aircraft noise contour model: ANCON version 1," Tech. rep. dot-vntsc-faa-16-17, Federal Aviation Administration (FAA), July 2016.

[5] Nuic, A., Poles, D., and Mouillet, V., "BADA: An advanced aircraft performance model for present and future ATM systems," *INTERNATIONAL JOURNAL OF ADAPTIVE CONTROL AND SIGNAL PROCESSING*, 2010.

[6] Ollerhead, J., "The CAA aircraft noise contour model: ANCON version 1," Tech. rep. dora 9120, Civil Aviation Authority (CAA), January 1992.

[7] Torija, A. J., Self, R. H., and Flindell, I. H., "A model for the rapid assessment of the impact of aviation noise near airports," *The Journal of the Acoustical Society of America*, , No. 2, 2017, pp. 981–995.

[8] Smith, M. J. T., *Aircraft Noise*, Cambridge University Press, 1989.

[9] Stewart, E. C., and Carson, T. M., "Simple method for prediction of aircraft noise contours," *J. Aircraft*, 1980, pp. 828–830.

[10] Synodinos, A. P., "A new framework for estimating noise impact of novel aircraft," Ph.D. thesis, 2017.

[11] "Society of Automotive Engineers: Procedure for the Calculation of Aircraft Noise in the Vicinity of Airports," Tech. Rep. 1845, SAE AIR, 1981.

[12] "AIR-5662," Tech. rep., Society of Automotive Engineers, 2006.

[13] Krebs, W., Butikofer, R., Pluss, S., and Thomann, G., "Spectral three-dimensional sound directivity models for fixed wing aircraft," *Acta Acustica united with Acustica*, 2006, pp. 269–277.

[14] Krebsand, W., Bütikofer, R., Plüss, S., and Thomann, G., "Modeling of Three-Dimensional Sound Directivity Patterns of Helicopters," Vol. 89, No. 273 – 279, 2003.

[15] Mobley, F. S., "Further development of 3-D rotary-wing acoustic directivity using spherical harmonic representation," Ph.D. thesis, 2012.

[16] "Helicopter Noise Exposure curves for use in Environmental impact assessment," Tech. rep. report no. faa-ee-82-16, Federal Aviation Administration(FAA), November 1982.